# Particle size, morphology and phase transitions in hydrothermally produced $VO_2$(D)

Diana Teixeira [¥ §], Raul Quesada-Cabrera [¥], Michael J. Powell [¥], G. K. L Goh[§], G. Sankar [¥], I. P. Parkin [¥], R. G. Palgrave [¥]

[¥] Department of Chemistry. Materials Chemistry Centre, University College London, 20 Gordon St. London WC1H 0AJ, United Kingdom.
[§] Institute of Materials Research and Engineering, Agency for Science, Technology and Research (A*STAR). 2 Fusionopolis Way. Singapore 138634

Corresponding author: *r.palgrave@ucl.ac.u

## Abstract

Different morphologies and sizes of $VO_2$(D) particles were synthetised via hydrothermal synthesis using ammonium metavanadate (${NH_4VO_3}$) or vanadium pentoxide ($V_2O_5$) as the vanadium precursors . By adjusting the vanadium precursors concentration and the pH of the starting solution a variety of morphologies and sizes of $VO_2$(D) particles from 20 nm to 3 µm could be produced. Flower-shape morphology was obtained under strongly acidic conditions, passing through star-shape particles of 1 µm at pH 2.5 and finally obtaining homogeneous round balls of around 3 µm at pH 6.9. Nanoparticles were produced hydrothermally using $V_2O_5$ as a precursor and hydrazine as a reducing agent. The transition temperature from $VO_2$(D) to thermochromic $VO_2$(R) in micron scale particles occurred at 350 °C under vacuum. However, nanoparticles of $VO_2$(D) had a significantly lower $VO_2$(D) to thermochromic $VO_2$(R) transition temperature of 165 $^{o}$C after annealing during only a few minutes. This is, to our knowledge, the lowest annealing temperature and time reported in the literature in order to obtain a thermochromic $VO_2$ material via another $VO_2$ phase.

After conversion of $VO_2$(D) *microparticles* to thermochromic $VO_2$(R), the metal to insulator transition temperature is 61± 1 °C for the heating cycle and 53± 1 °C for the cooling cycle. However, $VO_2$(R) *nanoparticles* showed a significantly reduced metal insulator transition of 59 ± 1 °C and 42 ± 1 °C for the cooling cycle lower than that reported in the literature for bulk $VO_2$. This is important due to the need to have a compound with a switching temperature closer to room temperature to be used in smart windows devices for energy consumption.

W-$VO_2$(D) star shape microparticles samples were prepared using 2-7 at% of dopant (using ammonium metavanadate as a precursor), although unexpectedly this does not seem to be a viable route to a reduced metal to insulator transition in this system.

**Keywords:** $VO_2$ (D), Thermochromic, pH, Morphology

## 1. Introduction

$VO_2$ has been investigated for a wide range of technological applications, including optical and electrical switching devices, multifunctional spintronics,[1] IR sensors and vision equipment, as coatings to prevent detection by reducing IR transmittance of blackbody emitters [2], to missile seeker sensors, and various other applications [3]. $VO_2$ nanorods have been used to prepare Li-ion batteries with a discharge capacity of 152 mA h/g [4]. W-doped $VO_2$(B) nanobelts are used in supercapacitors [5]. $VO_2$ nano-flowers were synthetized by Kang et al. for energy-storage devices and supercapacitors [6]. $TiO_2/VO_2$ *nanofibers* are reported to photocatalyze the degradation of pollutants from wastewater by Zhao et al. [7] $VO_2$(B) nanosheets were fabricated as cathode electrode presenting a high initial discharge and stable cyclability compared to bulk $VO_2$(B) as Want et al. reported in their work [8].

$VO_2$ has also been widely studied for architectural applications due to its thermochromic properties: $VO_2$ displays a reversible phase transition from a low temperature, monoclinic insulating phase, $VO_2$(M) to a high temperature, rutile, metallic phase, $VO_2$(R) at 68 °C.[9] This metal to semiconductor phase transition (MST) is associated with an increase in reflectivity in the near infrared which has led to the use of $VO_2$ as a thermochromic material, able to change its optical properties with temperature. Specifically, $VO_2$ films coated onto windows can actively switch between a high IR transmittance state below the MST temperature to a low IR transmittance state above the MST temperature.

The transition temperature of undoped $VO_2$(M) is 68 °C, which is too high for solar control coating applications. The transition temperature, however, can be reduced by doping with W, Ti, Mg or other ions; W doping is the most effective dopant, with a reduction of ~25 °C per at.% W incorporated. Therefore, doping is seen as an effective method to achieve $T_c$ in the optimum range for thermochromic windows.[10] [11] [12] Being able to reduce the phase transition temperature, towards room temperature, would allow for the maximum energy saving potential of the solar control coatings.

Vanadium dioxide ($VO_2$) has a well-known range of stable phases, such as $VO_2$(M) and $VO_2$(R), as well as metastable phases, such as $VO_2$(A), $VO_2$(B) and $VO_2$(C).[13] [14] Most of these phases consist of octahedrally coordinated $V^{4+}$ ions with different linkages of octahedra leading to the different crystal structures.[15] $VO_2$(A) has a MST temperature of 162 °C. The solid has a good thermal stability and oxidation resistance in air below 408 °C.[16] $VO_2$(B) has been commonly used as a convenient route to achieving $VO_2$(M) phase by annealing at 450 °C or above under an inert atmosphere.[17]

$VO_2$(D) is a newly discovered meta-stable phase[18] [17] that has gained attention in the $VO_2$ field as it allows the direct transition to $VO_2$(M) at relatively low temperatures (250 - 400 °C).[13] [18] Moreover, once the monoclinic phase is obtained from the $VO_2$(D) phase, the MST temperature of the resulting $VO_2$(M) material is lower (61 °C ) than that widely reported in the literature (68 °C).[13]

$VO_2$ can be produced from a wide range of methods, including atmospheric pressure chemical vapour deposition (APCVD),[1910] sputtering and spin coating [20] and, continuous hydrothermal flow synthesis [21] (CHFS) and hydrothermal synthesis [22] among others. Nevertheless, the challenge to find an easy, scalable and affordable process to produce $VO_2$(M) at low temperatures remains. A new approach to obtain $VO_2$(M) in one step via hydrothermal synthesis has been reported recently,[22] [11] however the process is not easily reproducible due to the strict control required over experimental conditions such as temperature, pressure, time, pH, etc.

Here we report the synthesis of $VO_2$(D) phase. A range of particle sizes, from nano to micro particles, were observed. The particle size and shape could be easily tailored by varying the pH, Furthermore, when in the form of nanoparticles, the $VO_2$(D) to (M) phase transition could be achieved at annealing temperatures as low as 165 °C, significantly lower that previous reports on the $VO_2$(D) to (M) phase transformation (*ca*. 400 °C). Moreover, the $VO_2$(R) particles thus produced show a lower thermochromic transition temperature than expected for bulk ~~undoped~~ vanadium dioxide. Finally we highlight the importance of particle size in controlling the phase behaviour of this important material. The advantages of producing nanoparticles of $VO_2$ is that they can give superior luminous transmittance and solar energy transmittance modulation compare to $VO_2$ films, as is reported in the literature by S.-Y Li et al [23].

## 2. Experimental section

### 2.1 Synthesis of $VO_2$(D) microparticles.

All reagents were obtained from Sigma Aldrich except for sodium hydroxide which was purchased from Alfa Aesar and were used without any further purification. In a typical reaction 0.625 g [0.0024 mol] of ammonium metavanadate ($NH_4VO_3$), 2.52 g of oxalic acid ($C_2H_2O_4$) used as a reducing agent, and 0.5 g of polyvinylpyrrolidone (PVP) were mixed into 50 mL of deionized water with continuous stirring until a green solution was obtained, indicating the presence of $V^3$ in the solution. The pH of the solution was adjusted using NaOH (1 M) (**Table *1***). The hydrothermal treatment was carried out using 27 mL of the resultant solution into a 45 mL Teflon lined autoclave and heated at 220 °C for 24 hours. Further studies were carried out using W-doped $VO_2$(D) microparticles synthesised using 2-7 at% of $WCl_4$ (relative to the vanadium precursor) added to the initial solution. The reaction conditions were the same used for the undoped samples. After hydrothermal synthesis, particles were filtered and washed with deionized water and ethanol.

**Table 1.** Sample names and descriptions for $VO_2$ powders synthesized by the reaction between $NH_4VO_3$ and $C_2H_2O_4$ in water. NaOH was used to adjust the pH of the starting solution. All samples were synthesized *via* hydrothermal treatment for 24 hours at 220 °C

| *Sample* | *pH of starting solution* |
|---|---|
| S01 | 0.65 |
| S02 | 0.98 |
| S03 | 1.05 |
| S04 | 1.52 |
| S05 | 2.5 |
| S06 | 3.51 |
| S07 | 4.6 |
| S08 | 5.5 |
| S09 | 6.91 |

### 2.2 Synthesis of $VO_2$(D) nanoparticles

To prepare the $VO_2$(D) nanoparticles, 0.45 g [0.0024 mol] of vanadium pentoxide ($V_2O_5$), 0.75 ml of sulfuric acid ($H_2SO_4$) and 0.25 ml of hydrazine hydrate were added to 10 mL of deionized water and stirred for a 3-5 minutes. The pH of the solution was adjusted to 6.6 – 6.9 using NaOH (1 M) and finally the solution was centrifuged to obtain a grey paste. The grey paste was dissolved in 19 mL of DI water and poured into a 45 mL teflon lined autoclave and heated to 240 °C for 48 hours. The product was isolated by centrifugation and washed with deionized water and ethanol.

In **Table *2*** the conditions used to prepare the $VO_2$(D) nanoparticles are stated. The pH range must be controlled within a narrow range to avoid an undesired phase. Three samples are presented here to show the pH range that can be used.

**Table 2**. Sample names and descriptions for $VO_2$ powders synthesized by the reaction between $V_2O_5$ and $H_2SO_4$ in water. NaOH was used to adjust the pH of the solution. Samples were synthesized *via* hydrothermal synthesis for 48 hours at 240 °C

| *Sample* | *pH of starting solution* |
|---|---|
| S16 | 6.62 |
| S17 | 6.75 |
| S18 | 6.84 |

### 2.3 Materials characterisation.

X-ray diffraction studies were carried out using a D8 GADDS Bruker diffractometer, utilising Cu K$\alpha$ radiation ($\lambda$= 1.541 Å) between 10 to 60, 2ϴ. Field Emission Scanning Electron Microscope (FESEM) analysis were performed using a JEOL JSM-6700Ff instrument with an accelerating voltage of 5 Kev and Transmission Electron Microscopy (TEM) analysis were taken using a Phillips CM300 FEG TEM, operated at 300 kV. Differential scanning calorimetry (DSC) analysis was obtained on a DSC 1 instrument from Mettler Toledo. These experiments were carried out between 0–300 °C under controlled nitrogen atmosphere with a heating ramp of 5 °C/min. Raman spectroscopy was performed using a Renishaw 1000 spectrometer with a 633 nm laser. The equipment was calibrated using a silicon reference.

## 3. Results and discussion

### 3.1 $VO_2$ powder characterization

$VO_2$ microparticles were produced through hydrothermal reaction of ammonium metavanadate with oxalic acid in the presence of polyvinylpyrrolidone (PVP). Adjusting the pH of the initial reactant mixture with 1.0M NaOH proved to be an easy and reproducible route to obtain microparticles of the $VO_2$(D) phase with different morphologies. The conditions used in the $VO_2$(D) microparticle synthesis are summarized in **Table *1***.

Figure 1 shows the XRD pattern of the prepared $VO_2$(D) phase using $NH_4VO_3$ as a precursor with different pH of the starting solution. All peaks shown in the as-prepared samples are indexed to the D phase of $VO_2$. In Figure 1 it is also presented the $VO_2$(D) pattern reported in the literature for comparison purposes. All the $VO_2$(D) peaks of the prepared samples match with the literature pattern [17].

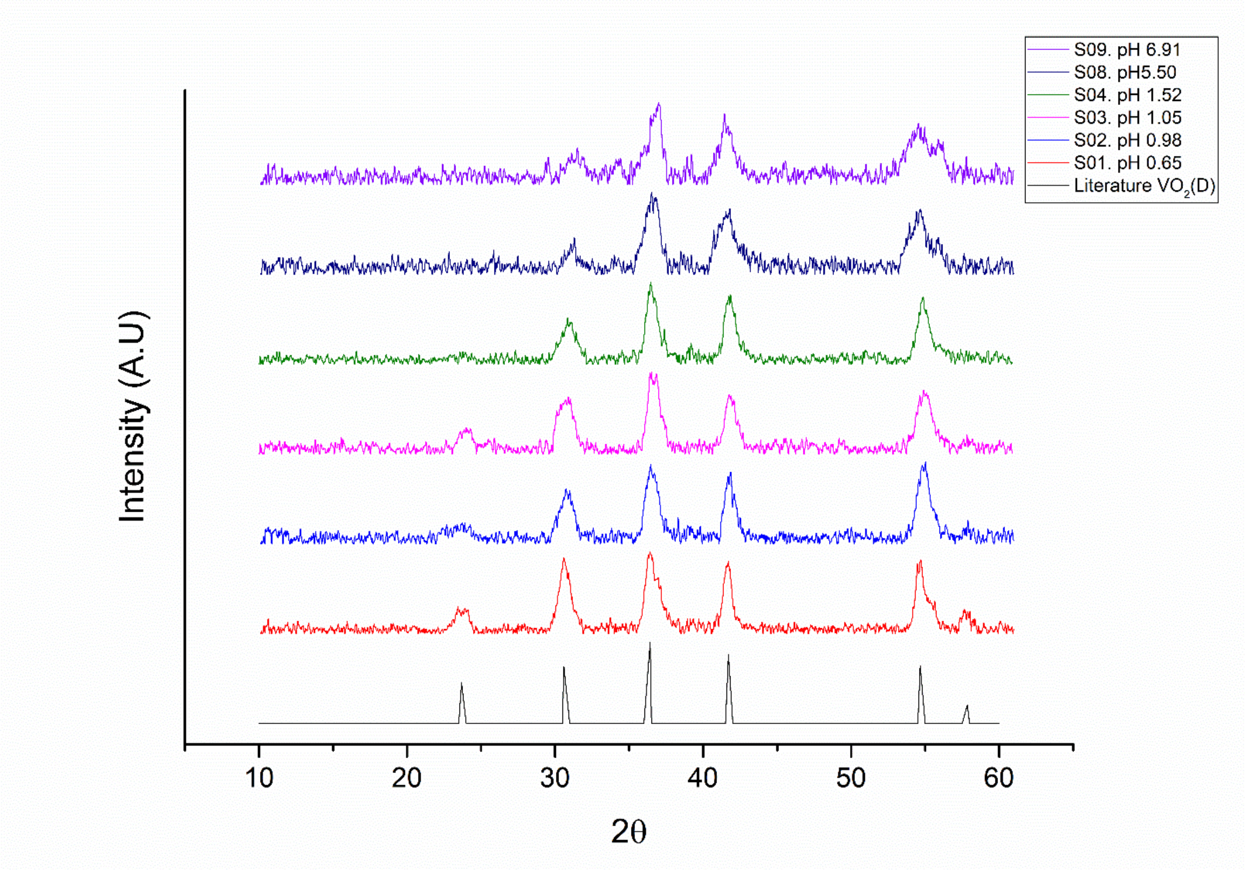

*Figure 1. (a) XRD patterns of the $VO_2$(D) microparticles as synthesised from ammonium metavanadate precursor under different pH conditions. A reference XRD pattern of $VO_2$(D) has been included from the literature.*[17]

$VO_2$(D) nanoparticles (20-40 nm) were obtained by hydrothermal synthesis using $V_2O_5$, hydrazine hydrate and sulfuric acid as starting reagents. In this case, changing the pH appears to affect the phase of vanadium oxide produced rather than the morphology. $VO_2$(D) is formed only at pH between 6.6 – 6.9, outside this range, other phases, $VO_2$(B) and $VO_2$(A), or mixed phases of $VO_2$ are obtained.

Figure 2 shows the XRD of three as-prepared samples of $VO_2$(D) nanoparticles with different pH compared to the $VO_2$(D) pattern reported in the literature [17].

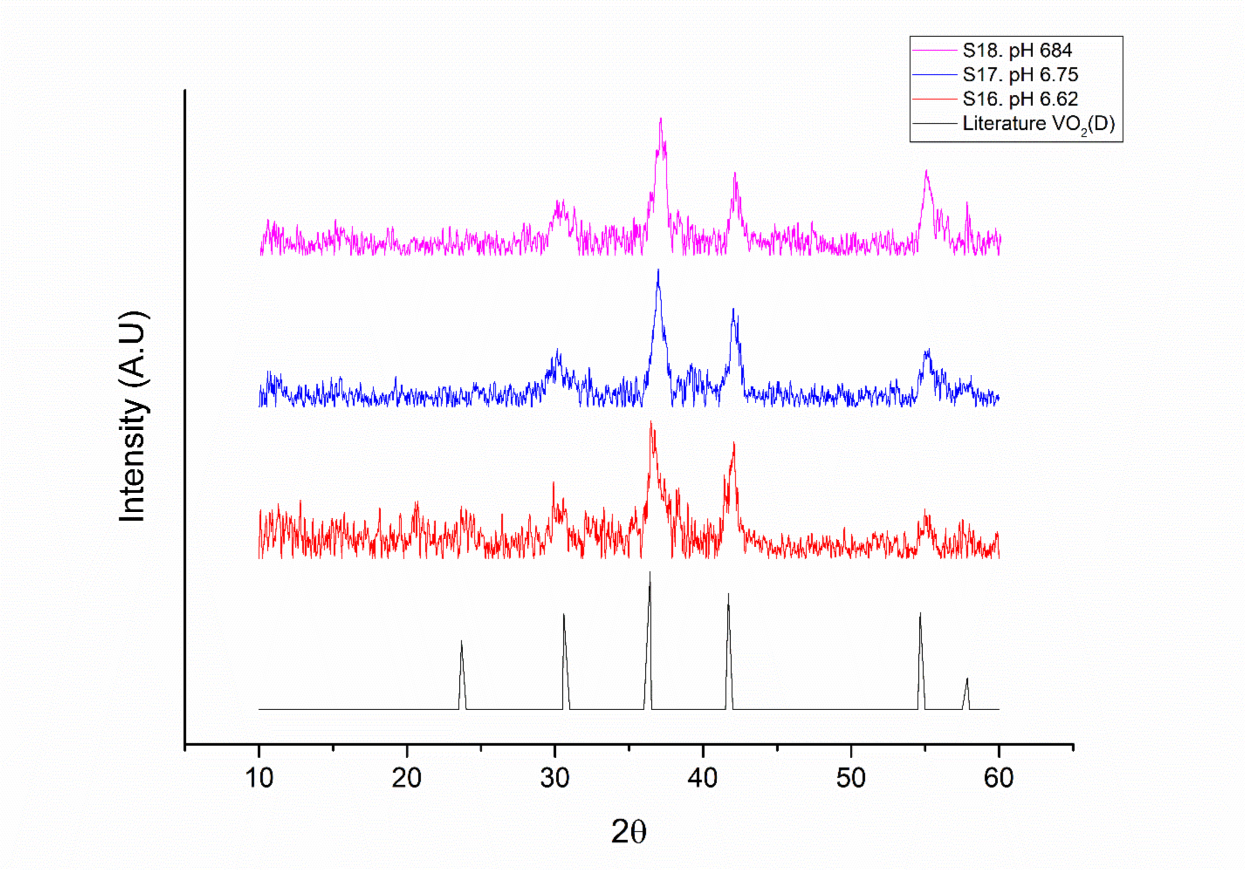

*Figure 2 XRD pattern of the prepared samples using vanadium pentoxide as a precursor and NaOH to adjust the pH of the solution. All peaks correspond to the $VO_2$(D) phase shown in the literature* [17]

Raman spectroscopy was performed to the as-prepared samples with different pH of the starting solution. The result obtained in all cases was the typical Raman spectroscopy bands for $V_2O_5$ [24]. When $VO_2$ powder is exposed to air the surface of the sample tends to oxidize, thus when running surface analysis as Raman, it is not unusual to obtain $V_2O_5$ in the results, which represent 5+ oxidation state, the most stable one. In this case, Raman spectroscopy bands show typical bands of $V_2O_5$, indicating that some degree of oxidation has taken place in our samples.

SEM images of the $VO_2$ microparticles are shown in Figure 3, as can be seen, increasing the pH of the starting solution without changing any other condition results in a growth of the particle size, and also a change in morphology. At pH 0.65 a “flower shape” morphology made of small attached long particles is seen, while moving towards neutral pH, larger smooth spheres are obtained.

In the present work ammonium metavanadate react with oxalic acid to produce vanadium (IV) oxide, carbon monoxide and carbon dioxide as can be seen in equations (1), (2) and (3), this solution have an acid pH, thus, small particle size, good homogeneity and low agglomeration is expected (and obtained in the as prepared samples)

$$2NH_4VO_3 + 4C_2H_2O_4 \rightarrow (NH_4)_2[(VO)_2(C_2O_4)_3] + 2CO_2 + 4H_2O \quad \textbf{(1)}$$

$$(NH_4)_2[(VO)_2(C_2O_4)_3] \rightarrow 2VOC_2O_4 + 2NH_3 + CO + CO_2 + H_2O \quad \textbf{(2)}$$

$$VOC_2O_4 \rightarrow VO_2 + CO + CO_2 \quad \textbf{(3)}$$

However, when adding the sodium hydroxide in the process to adjust the pH of the solution, we are also producing sodium orthovanadate, ammonia and water, as can be seen in equation (4). This could affect the homogeneity of particles, due to greater agglomeration and growth of the particles. This explains the growth and the agglomeration of our particles due to the increase of the pH of the initial solution.

$$NH_4VO_3 + 3NaOH \rightarrow Na_3VO_4 + NH_3 + 2H_2 \quad \textbf{(4)}$$

The change in the morphology and size due to simply changes in pH is interesting as the $VO_2$(D) phase can be used for different applications depending on the morphology and size.

The pH of the starting precursor solution had a dramatic effect on the morphology observed in the synthesized $VO_2$ particles Figure 3. At a pH of 0.65, Figure 3(a), a star/flower shape can be seen, similar to the desert rose formation of minerals. This morphology has been previously observed in other hydrothermally produced materials [25] [4]. Increasing the pH of the starting solution to 0.98, Figure 3(b), causes the flower shape to disappear and a series of circular fused plates can be seen, apparently formed by small long particles well attached one to the other, almost forming a solid sphere. At a pH of 1.05, Figure 3(c), the particles appear more spherical, with ridges present on the surface of the particles. Further increasing the pH to 1.52, Figure 3(d), results in the formation of small cross-shape structures that are well define can be seen to overlap to form larger structures. At a pH of 2.50, Figure 3(e), the individual well-defined structures can still be seen, however it seems like their growth rate has being retarded. At pH values above 3.5, the particle shapes become more homogeneous, eventually adopting a sphere like shape. This can be seen in Figure 3(f), (g) and (h), where the higher pH of the starting precursor solution can be clearly seen to prevent the formation of the smaller crystallite structures.

Particle sizes range from 1 µm at the most acidic pH to ~4 µm when pH is close to neutral. It is interesting that the morphology in most of the cases has a round shape but always present a "Ball-shape" made of small long rods attached, the round shape can be attributed to the use of PVP as this has been reported as a crystal growth modifier [17]. The presence of PVP in this experiments seems to be essential in the formation of $VO_2$(D) phase as reported by Liu Liang et all [17] if no PVP is added the product shows a pure $VO_2$(B) phase.

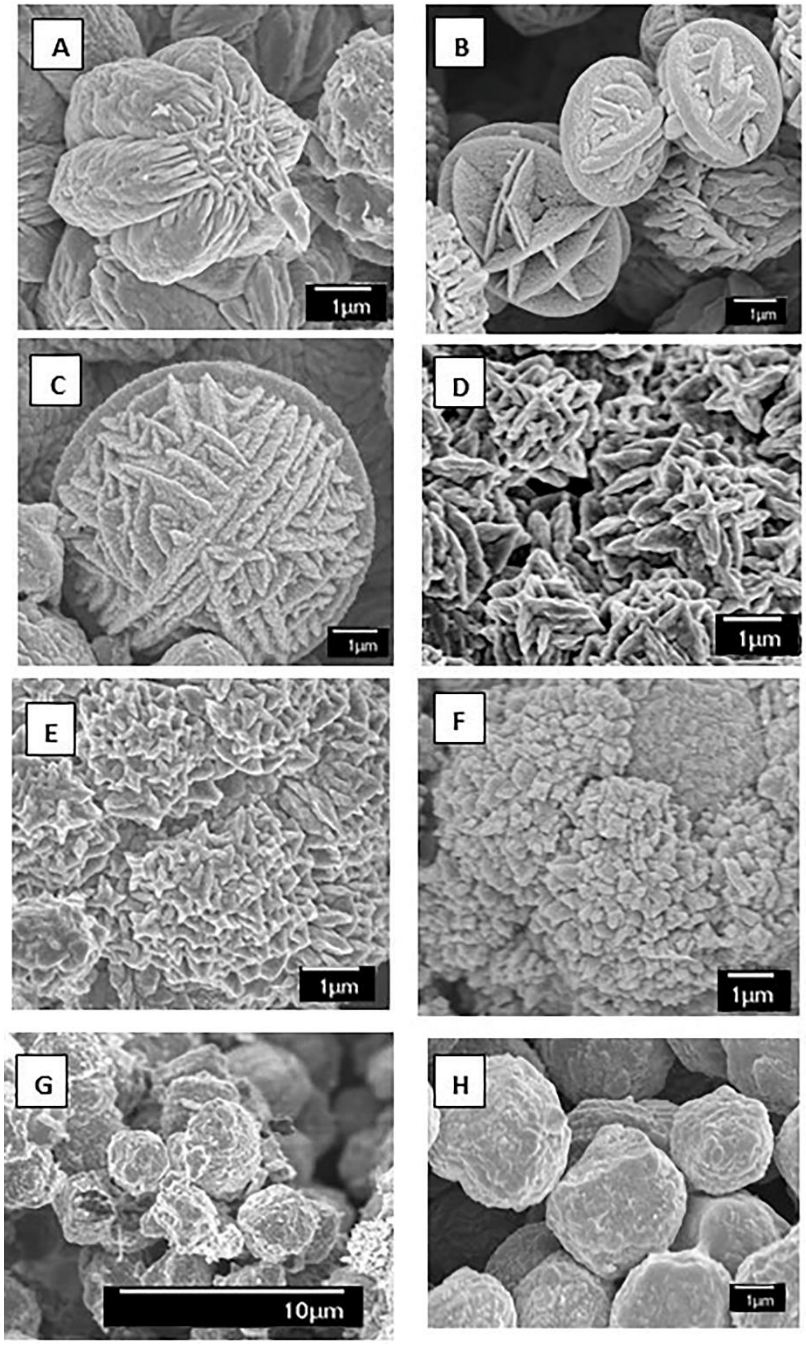

*Figure 3 SEM of the prepared samples using ammonium metavanadate as a precursor with different pH: (A) 0.65 (B) 0.98 (C) 1.05 (D) 1.52 (E) 2.50 (F) 3.51 (G) 4.60 (H) 6.91*

The nanoparticles of the $VO_2$(D) were prepared using $V_2O_5$ as a precursor. In Figure 4 SEM and TEM images of the as-prepared samples can be seen. The particle size is around 20-40 nm and present mainly a round shape. The $VO_2$(D) nanoparticles do not show any growth after heat treatment to convert to $VO_2$(R), meaning that the final products remain as nanoparticles.

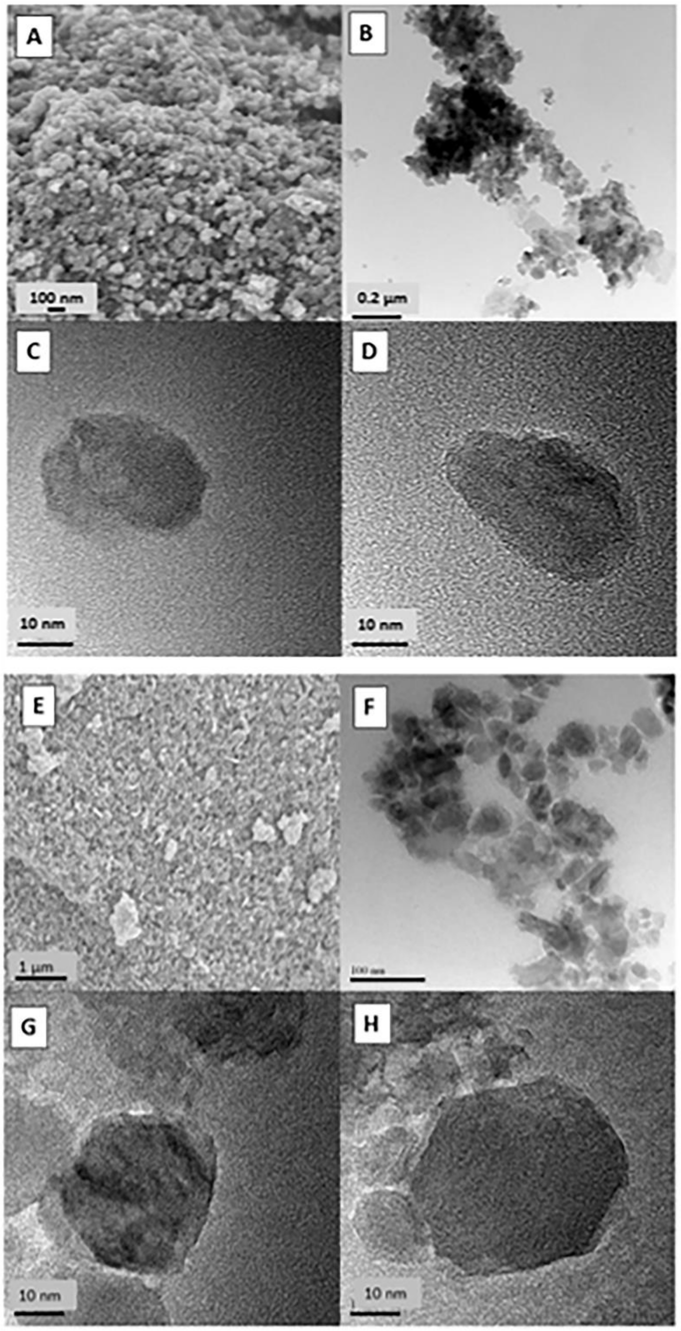

*Figure 4 (a) SEM image of sample 16 (b, c, d) TEM images of sample 16 (e) SEM image of sample 17 (f, g, h) TEM images of sample 17*

Hydrazine is well known to promote nanoparticles formation as it can coordinate to metal ions during hydrothermal synthesis [26]. Hence we believe that hydrazine plays a critical role in the production of $VO_2$(D) nanoparticles here.

### 3.2 Functional properties

The typical approach to obtained $VO_2$(R) for thermochromic applications is by annealing $VO_2$(B) phase in the vacuum at temperatures that range between 420-700 ºC.[27] [28] The actual transformation temperature depends on the morphology of the $VO_2$(B) particles, we have notice in this work that nanoparticles of $VO_2$(D) require less time/temperature to transform into $VO_2$(M) than $VO_2$(D) microparticles. Importantly, the $VO_2$(D) phase can be converted to thermochromic $VO_2$(R) by thermal treatment at temperatures as low as 250 ºC [29] This is highly significant, as low temperature conversion allows preservation of the nanostructure of the parent phase, and as mention before, nanostructures give superior luminous transmittance and solar energy transmittance modulation, being this a key point of the production of thermochromic $VO_2$. The nano- and microparticles produced in this work showed significantly different phase transition behaviour. DSC was attempted to study the $VO_2(D)\rightarrow VO_2(R)$ transition in our microparticles. However, the maximum temperature of our DSC was 300 °C, and the desired transition did not occur in this temperature range. It was found that by annealing in vacuum the $VO_2(D)\rightarrow VO_2(M)$ transition occurred in our microparticles around 350 ºC. Once converted to thermochromic $VO_2$(R), cooling to room temperature will cause a further transition to $VO_2$(M). This $VO_2$(M) material was then subject to DSC to study the $VO_2(M)\rightarrow VO_2(R)$ transition, and the results are shown in Figure 5. All studied samples present the same $T_c$ to within 5 °C and for convenience only two samples are shown. As is shown in Figure 5 there is a slight difference between the critical temperature for each sample, this may be due to morphology. In general the $T_c$ is at 61 ± 3 °C for the heating cycle and 55 ± 2 °C for the cooling cycle, thus the thermal hysteresis width calculated from DSC is 6 ± 1 °C.

Reported DSC in the literature of $VO_2$(R) obtained in one step *via* hydrothermal synthesis shows a $T_c$ temperature at 65 °C for the heating cycle and 53.5 °C for the cooling sample [30], while samples of $VO_2$(R) obtained via $VO_2$(A) using hydrothermal synthesis method have a $T_c$ for the heating cycle of 69 °C and 61 °C for the cooling sample[31]. Samples of $VO_2$(R) obtained via $VO_2$(D) have a $T_c$ 67.5 °C for the heating cycle and 59.7 °C for the cooling cycle [13], while our results, using the same method present a $T_c$ for the heating cycle at 61 ± 3 °C and 55 ± 2 °C for the cooling cycle, this represents 4-6 °C lower than reported previously. ~~The difference may be due to particle size and/or strain effect on our particles~~. The difference can be explained due to particle size and strain effect on our samples, it has to be noted that the microparticles shown here are composed by accumulation of nanoparticles.

In the literature Lopez et at reported the fabrication of $VO_2$ nanoparticles via Ion implantation method, in their work it is demonstrated that the transition temperature it is decreased due particle size effects and moreover as a result of defects in the $VO_2$ that causes nucleation spots for the phase transition[32].

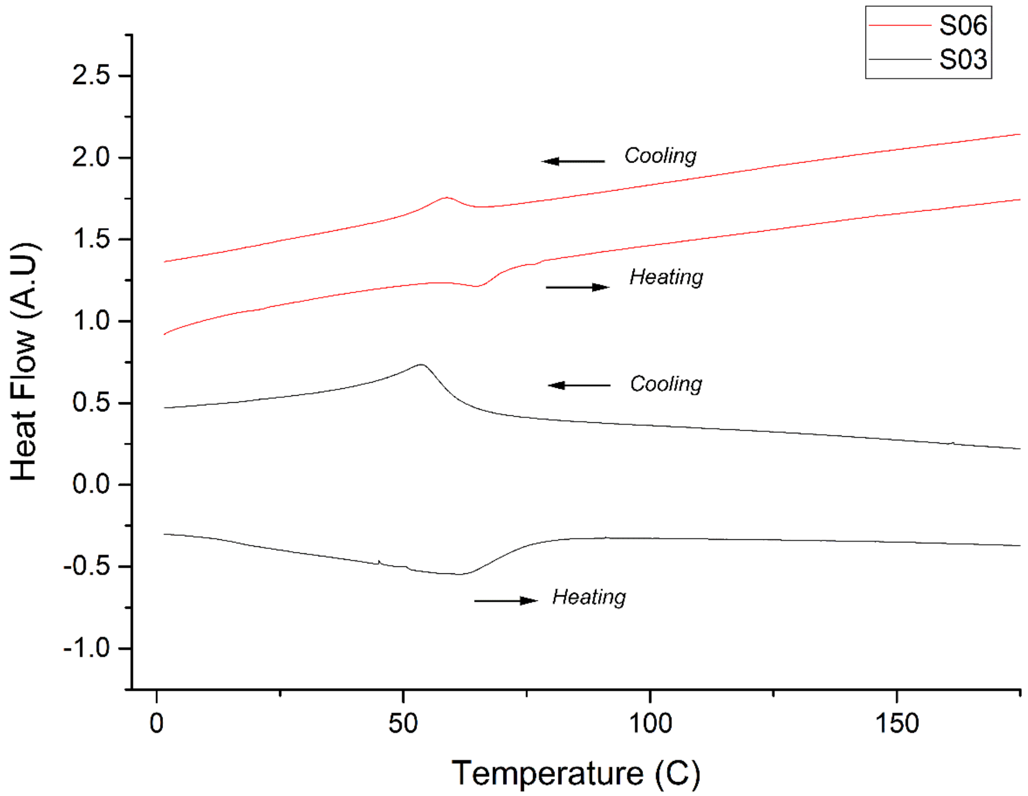

*Figure 5 DSC curves of $VO_2$(R) obtained via micro-$VO_2$(D) after heat treatment*

Phase nucleation is reported to be due to vacancies, substitutions, etc. [33], Oxygen vacancies are usually reported in the literature as defects on nanostructure surfaces [34], therefore while the size of the particles decreased, the surface ratio increase, consequently the nucleation defect density is higher in smaller particles causing the diminution of the transition temperature in the as-prepared nanoparticles, compared to the as-prepared microparticles.

In Table 3 DSC measurementes of critical temperatures for the mentioned $VO_2$(R) reported in the literature and in the present work are shown.

*Table 3. Comparison of DSC transition temperatures for heating and cooling cycles of $VO_2$(R)(to $VO_2$(M)).*

| **Process** | **$T_c$ heating cycle (°C)** | **$T_c$ cooling sample (°C)** | **Hysteresis (°C)** |
|---|---|---|---|
| $VO_2$ (R) One step hydrothermal synthesis [11] | 65 | 53.5 | 12.5 |
| $VO_2$(B) → $VO_2$(R) hydrothermal synthesis [35] | 68.75 | 59.77 | 8.98 |
| $VO_2$(D) → $VO_2$(R) Hydrothermal synthesis [29] | 67.5 | 57.9 | 9.6 |
| $VO_2$(D) → $VO_2$(R) hydrothermal synthesis (present work) | 61±3 | 55±2 | 8 |

Tungsten doped $VO_2$(D) microparticles samples were synthetized in order to study the change in the transition temperature once the rutile phase is obtained after heat treatment of the prepared sample. Is well known in the literature that the addition of tungsten to the vanadium thermochromic samples decrease the transition temperature. In our case samples were doped with 2, 3 and 4 at% of tunsgten (IV) chloride.

In Figure 6 is shown the DSC of three tungsten doped (2, 3 and 4 at%) $VO_2$(M) samples, obtained via $VO_2$(D). In all three samples the $T_c$ for the heating cycle is at 62 ± 1 °C and the $T_c$ for the cooling cycle in all cases is at 52 ± 1 °C. It is surprising that there is no significant change in the transition temperature as expected. It appears as if pre doping of $VO_2$(D) particles with W is not an effective way to lower the $T_c$ in subsequently porduced $VO_2$(M); our esults in fact suggest that W is not incorporated into the $VO_2$(D) lattice using the hydrothermal approach used here, see suplimentary information for full details of W doping experiments.

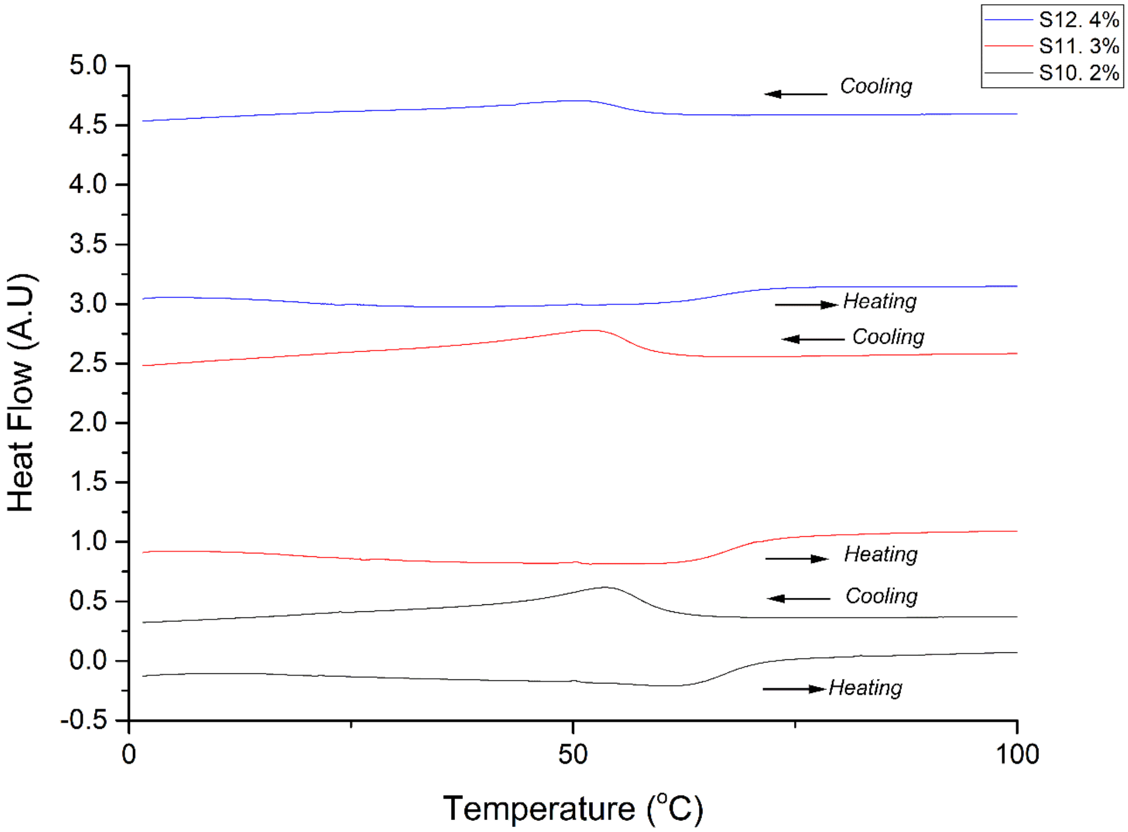

*Figure 6 DSC curves of tungsten dope $VO_2$(R) obtained via tungsten dope micro- $VO_2$(D) after heat treatment*

As discussed above, $VO_2$(D) microparticles samples required annealing at 350°C to obtain $VO_2$(R). However for $VO_2$(D) nanoparticles, a much lower annealing temperature is required. DSC illustrating the phase transitions occurring on annealing under $N_2$ of $VO_2$(D) nanoparticles is shown in Figure 7. In the first heating cycle of the as made materials, the first significant feature in the DSC curve occurs at 163 ± 2 °C, where a strong endothermic peak is seen. This is assigned to the $VO_2(D)\rightarrow VO_2(R)$ transition. No further transitions are seen on heating up to 300 °C. Upon the first cooling cycle, no feature is seen around 163 °C, showing that the phase transition seen in the heating cycle is irreversible. Upon further cooling, an exothermic peak is seen at 42 ± 1 °C; this is assigned to the $VO_2(R)\rightarrow VO_2(M)$ transition. On the second heating cycle, the system displays typical thermochromic behaviour. An endotherm peak is now seen at 59 ± 1 °C ($VO_2$(M)—$VO_2$(R)). No further signals are seen up to 300°C. On the second cooling cycle, an exotherm peak is again seen at 42 ± 1 °C ($VO_2$(R)—$VO_2$(M)). It is noteworthy that in these samples the $VO_2(D)\rightarrow VO_2(R)$ transition temperature of 163 °C is significantly lower than previous reported (250 °C),[5] which we attribute to the small size of the particles. The thermochromic material thus produced also shows a lower MST temperature than expected from bulk ~~undoped~~ vanadium dioxide. This has also been seen previously with nanoscale $VO_2$ [25].

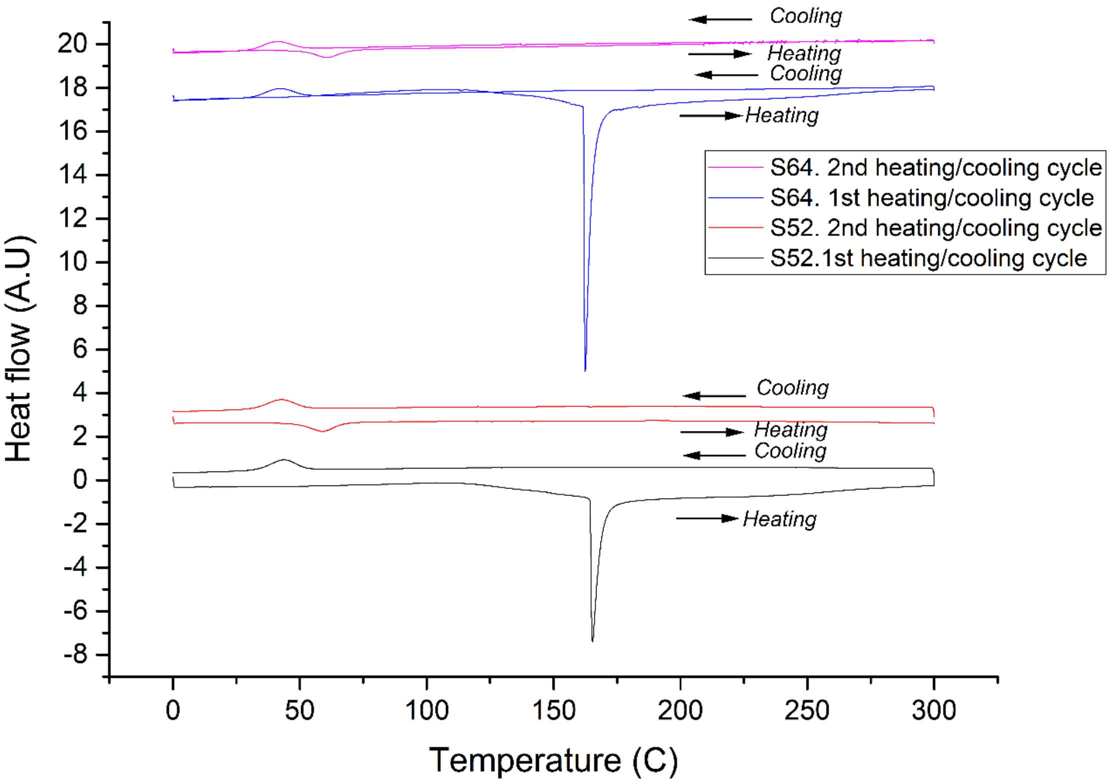

*Figure 7 DSC curves of $VO_2$(R) obtained via nano- $VO_2$(D) samples showing: the transition from D to R phase and then, the reversible thermochromic behaviour of $VO_2$(R)*

## Conclusion

$VO_2$(D) microparticles were synthesised using $NH_4VO_3$ and oxalic acid as a precursor and reducing agent respectively via a hydrothermal synthesis reaction. We demonstrate in this work that it is possible to obtain pure $VO_2$(D) with different morphologies simply changing the pH of the starting solution using NaOH at 1M concentration. A phase transformation from D to M is possible at 350 °C under vacuum obtaining pure monoclinic phase with MST reported at 61 °C for the heating cycle and 55 °C for the cooling cycle.

W doping of $VO_2$(D) microparticles was attempted, yet the MST temperature for each nominally doped sample was unchanged from undoped $VO_2$, signalling that W doping of $VO_2$(D) followed by conversion into $VO_2$(R) does not appear to be successful.

$VO_2$(D) nanoparticles were synthetized using vanadium pentoxide and sulfuric acid as a precursor and reducing agent respectively. The size of the obtained particles oscillates between 20 to 40 nm. To obtain $VO_2$(M) in this case it is required to heat treat the sample at 165 °C for a few minutes under nitrogen atmosphere. After the samples are heat treated a fully thermochromic sample is obtained with a MST for the heating cycle at 59 °C and 42 °C for the cooling cycle. This is the lowest $VO_2$(D)→$VO_2$(R) transition temperature reported ~~for undoped $VO_2$~~ in the literature, and shows the importance of particle size on phase transition temperatures. In addition the reported MST temperature in this work for $VO_2$(M) nanoparticles obtained from $VO_2$(D) is lower than reported for bulk ~~undoped~~ $VO_2$. We attribute this to the particle size and strain in nanoparticles of $VO_2$(R) produced from $VO_2$(D).

1 R. Molaei, R. Bayati, S. Nori, D. Kumar, J. T. Prater and J. Narayan, *Appl. Phys. Lett.*, 2013, **103**, 2–6.

2 C. Moffatt and A. Wigstein, *Sol-gel synthesis of VO 2 thin films and the effects of W and Re doping*, 2005.

3 H. Jerominek, F. Picard, N. R. Swart, M. Renaud, M. Lévesque, M. Lehoux, S. Castonguay, M. Pelletier, G. Bilodeau, D. Audet, T. D. Pope and P. Lambert, *Proc. SPIE 2746*, 1996, 60–71.

4 C. V Subba, E. H. Walker, S. A. W. Sr, Q. L. Williams and R. R. Kalluru, *Curr. Appl. Phys.*, 2009, **9**, 1195–1198.

5 Y. Zhang and Y. Huang, *Mater. Lett.*, 2016, **182**, 285–288.

6 X. Juan, J. Ming, X. Wen, F. Rui and Y. Xin, *Ceram. Int.*, 2016, **42**, 7883–7887.

7 K. Zhao, L. Teng, Y. Tang and X. Chen, *Ceram. Int.*, 2014, **40**, 15335–15340.

8 Q. Wang, J. Pan, M. Li, Y. Luo, H. Wu, L. Zhong and G. Li, *J. Mater. Sci. Technol.*, 2015, **31**, 630–633.

9 Z. Chen, Y. Gao, L. Kang, C. Cao, S. Chen and H. Luo, *J. Mater. Chem. A*, 2014, **2**, 2718.

10 M. J. Powell, R. Quesada-cabrera, A. Taylor, D. Teixeira, I. Papakonstantinou, R. G. Palgrave, G. Sankar and I. P. Parkin, *Chem. Mater.*, 2016, **28**, 1369–1376.

11 J. Zhu, Y. Zhou, B. Wang, J. Zheng, S. Ji, H. Yao, H. Luo and P. Jin, *Appl. Mater. Interfaces*, 2015, **7**, 27796–27803.

12 Y. Gao, S. Wang, H. Luo, L. Dai, C. Cao, Y. Liu, Z. Chen and M. Kanehira, *Energy Environ. Sci.*, 2012, 6104–6110.

13 Z. Song, L. Zhang, F. Xia and N. A. S. Webster, *Inorg. Chem. Front.*, 2016, **3**, 1035–1042.

14 D. Hagrman, J. Zubieta, C. J. Warren, L. M. Meyer, M. M. J. Treacy and R. C. Haushalter, *J. Solid State Chem.*, 1998, **182**, 178–182.

15 J. H. Park, J. M. Coy, T. S. Kasirga, C. Huang, Z. Fei, S. Hunter and D. H. Cobden, *Nature*, 2013, **500**, 431–434.

16 Y. Zhang, X. Tan, C. Huang, C. Meng, Y. Zhang, X. Tan, C. Huang and C. Meng, *Mater. Res. Innov.*, 2016, **10**, 295–302.

17 L. Liu, F. Cao, T. Yao, Y. Xu, M. Zhou, B. Qu, B. Pan, C. Wu, S. Wei and Y. Xie, *New J. Chem.*, 2012, **36**, 619.

18 L. Zhong, M. Li, H. Wang, Y. Luo, J. Pan and G. Li, *CrystEngComm*, 2015, **17**, 5614–5619.

19 D. Louloudakis, D. Vernardou, E. Spanakis, S. Dokianakis, M. Panagopoulou, G. Raptis, E. Aperathitis, G. Kiriakidis, N. Katsarakis and E. Koudoumas, *Phys. status solidi C*, 2015, **860**, 856–860.

20 Y. Shimizu, K. Nagase, N. Miura and N. Yamazoe, *Jpn. J. Appl. Phys.*, 1990, **29**, 1708–1711.

21 M. J. Powell, P. Marchand, C. J. Denis, J. C. Bear, J. A. Darr and I. P. Parkin, *Nanoscale*, 2015, **7**, 18686–18693.

22 J. H. Son, J. Wei, D. Cobden, G. Cao and Y. Xia, *Chem. Mater.*, 2010, **22**, 3043–3050.

23 S. Y. Li, G. a. Niklasson and C. G. Granqvist, *J. Appl. Phys.*, 2010, **108**, 1–8.

24 C. Sanchez, J. Livage and G. Lucazeau, *J. Raman Spectrosc.*, 1982, **12**, 3–7.

25 B. Lei, W. Qin, G. Kang, C. Peng and J. Wu, *J. Am. Ceram. Soc.,* 2015, **1633**, 1626–1633.

26 H. Zhu, D. Yang, G. Yu and H. Zhang, *Nanotechnology*, 2006, **17**, 2386–2389.

27 C. Wang, X. Wang, P. Gong and T. Yao, *Chemosphere*, 2016, **149**, 358–365.

28 S. A. Corr, M. Grossman, Y. Shi, K. R. Heier, D. Stucky and R. Seshadri, *J. Mater. Chem.*, 2009, **2**, 4362–4367.

29 G. Zhengdong, Song; Liangmiao, Zhang; Fang, Xia; Nathan A. S., Webster; Jingchao, Song; Bin, Liu; Hongjie, Luoa; Yanfeng, *Inorg. Chem.*, 2016, **3**, 1035–1042.

30 W. Li, S. Ji, Y. Li, A. Huang, H. Luo and P. Jin, *RSC Adv.*, 2014, **4**, 13026.

31 S. Rao, A. Artemenko, C. Labrugere and M. Miclau, *J. Solid State Chem.*, 2014, **213**, 79–86.

32 R. Lopez, T. E. Haynes and L. A. Boatner, *Phys. Rev. B*, 2002, **65**, 1–5.

33 L. Hongwei, L. Junpeng, Z. Minrui, T. S. Hai, S. C. Haur, Z. Xinhai and K. Lin, *Opt. Express*, 2014, **22**, 30748–30755.

34 J. Jeong, N. Aetukuri, T. Graf, T. D. Schladt, M. G. Samant and S. S. P. Parkin, *Science (80-. ).*, 2013, **339**, 1402–1406.

35 M. Li, F. Kong, Y. Zhang and G. Li, *CrystEngComm*, 2011, **13**, 2204.